Chemical Physics Letters 691 (2018) 462–472

Contents lists available at ScienceDirect

Chemical Physics Letters

journal homepage: www.elsevier.com/locate/cplett

Frontiers article

Application of acoustic micro-resonators in quartz-enhanced photoacoustic spectroscopy for trace gas analysis

Huadan Zheng [a,b,c,1], Lei Dong [a,c,1,*], Hongpeng Wu [a,c], Xukun Yin [a,c], Liantuan Xiao [a,c], Suotang Jia [a,c], Robert F. Curl [d], Frank K. Tittel [b]

[a] State Key Laboratory of Quantum Optics and Quantum Optics Devices, Institute of Laser Spectroscopy, Shanxi University, Taiyuan 030006, China
[b] Department of Electrical and Computer Engineering, Rice University, Houston, TX 77005, USA
[c] Collaborative Innovation Center of Extreme Optics, Shanxi University, Taiyuan 030006, China
[d] Department of Chemistry, Rice University, Houston, TX 77005, USA

ARTICLE INFO

Article history:
Received 28 November 2017
In final form 5 December 2017
Available online 6 December 2017

Keywords:
Quartz enhanced photoacoustic spectroscopy
Quartz tuning fork
Acoustic micro-resonator
Gas sensing
Laser spectroscopy

ABSTRACT

During the past 15 years since the first report of quartz enhanced photoacoustic spectroscopy (QEPAS), QEPAS has become one of the leading optical techniques for trace chemical gas sensing. This paper is a review of the current state-of-the art of QEPAS. QEPAS based spectrophones with different acoustic micro-resonators (AmR) configurations employing both standard quartz tuning forks (QTFs) and custom-made QTFs are summarized and discussed in detail.

1. Introduction

Quartz tuning fork (QTF) oscillators were introduced in watches and clocks in order to significantly improve the timekeeping accuracy in the 1960 s. A standard watch QTF has a resonance frequency, $f = 2^{15}$ Hz (32,768 Hz) and a quality factor $Q > 80{,}000$ in a metallic vacuum encapsulation, which is a high Q factor piezoelectric element with a narrow full width at half maximum (FWHM) passband of <1 Hz [1]. QTFs in watches and clocks are made to vibrate by a small oscillating voltage applied to metal electrodes deposited on the surface of the quartz crystal via an electronic oscillator circuit. In 2002, a QTF was first used as the piezoelectric transducer to detect the sound waves induced by the photoacoustic effect due to molecular absorption of light energy, which is named quartz-enhanced photoacoustic spectroscopy (QEPAS) by Kostever [2–4].

In photoacoustic spectroscopy, the signal amplitude S can be expressed as:

$$S \propto \frac{Q \cdot P \cdot \alpha}{f} \tag{1}$$

where Q is the Q factor of the spectrophone, P is the pressure, α is the molecular absorption coefficient and f is the modulation frequency [3]. The high detection sensitivity of QEPAS benefits from the extremely high Q factor of the QTF, since a high Q factor corresponds to a long energy accumulation time [2]. A condition to ensure an optimum photoacoustic signal is that the vibrational to translation (V-T) relaxation rates should follow the modulation frequency f efficiently [5–7]. A significant advantage of QEPAS is the capacity of environmental noise immunity, compared to conventional photoacoustic spectroscopy (PAS) based on a wide band microphone [8–12]. The QTF is an acoustic quadrupole, which means that only the sound wave produced by the source located between the QTF prong spacing can drive the QTF prongs to vibrate in the opposite direction and produces an output electrical signal, while an external sound wave that pushes the QTF prongs to vibrate in the same direction produces no signals [2,3]. The QTF only responds to a sound wave modulated with the identical frequency as that of the QTF. The sampling gas volume required by the QEPAS sensor is <1 cm^3 due to the small size of the QTF [4].

In order to enhance the QEPAS sensor performance, acoustic micro-resonators (AmR) are configured with a QTF to confine the sound waves and increase the signal amplitude [13]. Typically, a

* Corresponding author at: State Key Laboratory of Quantum Optics and Quantum Optics Devices, Institute of Laser Spectroscopy, Shanxi University, Taiyuan 030006, China.
E-mail address: donglei@sxu.edu.cn (L. Dong).
[1] These authorship contributes equally to this work.

https://doi.org/10.1016/j.cplett.2017.12.006
0009-2614/

QTF plus an AmR is referred to as a QEPAS spectrophone. Benefiting from the continuous innovation and creativity of laser technology, light sources ranging from the ultraviolet (UV) region to the near infrared (NIR), mid infrared (MIR) and terahertz (THz) regions [14–50] have been applied to QEPAS sensor systems for atmospheric monitoring [51–58], medical diagnostics [59–61], accidental gas emissions [62–64], chemical analysis [65–72] and trace detection [73–79]. Different kinds of QEPAS spectrophones have been designed and developed to address various applications.

2. Typical QEPAS based sensor system

A typical QEPAS experimental sensor system based on a wavelength modulation technique is shown in Fig. 1 [80]. Due to the intrinsic QTF feature of a high Q factor, a slow ramp signal, typically ~10 to 100 mHz, was applied to the laser driver to tune the laser emission wavelength to cover the absorption line of a targeted analyte. A sinusoidal dither signal was added to the laser driver to modulate the laser wavelength with the modulation frequency of $f_0/2$, where f_0 was the QTF resonance frequency. The laser emission was focused between the QTF prong spacing by a fiber collimator or a focusing lens [81–83]. Any laser illumination on the QTF surfaces or prongs results in undesirable background noise. The QEPAS spectrophone was enclosed in a gas cell in which both the pressure and the gas flow rate can be controlled. An empirical gas flow rate in the QEPAS cell is <200 standard cubic centimeter per minute (sccm) in order to avoid flow noise. The sound wave, induced by the photoacoustic effect upon gas absorption, forces the QTF prongs to vibrate at its resonance frequency. The QTF output signal was processed first by a transimpedance pre-amplifier and then directed to a lock-in amplifier [81]. The lock-in amplifier operated in the 2f mode to demodulate the signals which were related to the target analytes. The signals from the lock-in amplifier can be collected by a DAQ (data acquisition) card and recorded by a personal computer. For incoherent light sources whose emission wavelength cannot be tuned, an amplitude modulation technique was applied to the QEPAS system, in which the light sources were modulated at the QTF resonance frequency f_0 and the lock-in amplifier demodulated the QTF signal in the 1f mode [14–17].

3. QEPAS spectrophone employing standard QTFs

Commercially available standard watch QTFs usually have the resonance frequency of 32.7 kHz and are enclosed in two kinds of metallic encapsulation in diameter × length: 3 × 8 mm and 2 × 6 mm. The 3 × 8 mm standard QTF with U-shaped crystal dimensions of 6 mm (length) × 1.4 mm (width) × 0.2 mm (thickness) and a QTF prong spacing of ~0.2 mm is widely used because of its larger prong spacing. Another commercially available QTF with lower resonance frequency of 30.72 kHz and nearly the same geometry was also employed in a QEPAS system reported by Ma [84–88]. The QEPAS signal is inversely proportional to the modulation frequency according to Eq. (1). Hence the QEPAS detection sensitivity can be improved by using QTFs with a lower frequency.

3.1. On-beam QEPAS configuration

The sound wave induced by the excitation of a laser beam is cylindrical with a relatively small amplitude. A linear equation can be used to describe the propagation of the photoacoustic sound wave [89]:

$$\partial_t^2 p(\mathrm{r},t) - v^2\nabla^2 p(\mathrm{r},t) = (\sigma - 1)\partial_t H(\mathrm{r},t) \quad (2)$$

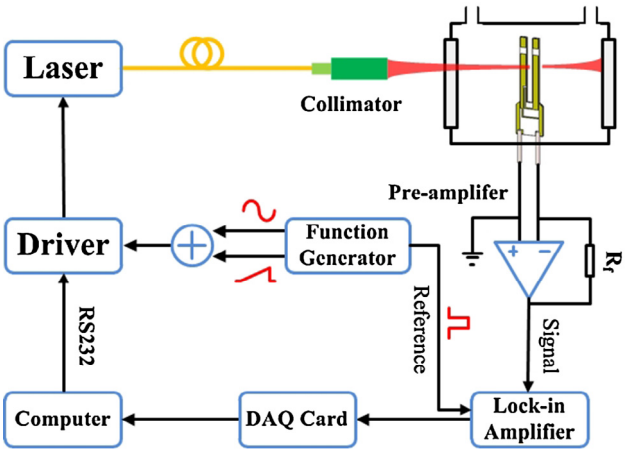

Fig. 1. Schematic of a typical QEPAS sensor system.

where p, v, σ and H are the sound pressure, velocity, the adiabatic coefficient of the gas, and the heat density deposited in the gas by light absorption, respectively. The sound wave propagation undergoes an attenuation of several centimetres due to air damping. However when the gas is confined within an acoustic resonator, the sound wave amplitude may increase considerably because of the constructive interference caused by the boundaries. Cylindrical micro tubes can be configured with the QTF acting as an AmR to enhance the photoacoustic signal.

Fig. 2(a) depicts the combination of a QTF with an AmR consisting of a pair of tubes made of stainless steel or silica [94]. The tubes are assembled perpendicularly to the QTF plane and positioned as close to the QTF as possible, but avoiding touching the QTF. Theoretical simulation and experimental studies verified that the optimal distance between the end of the tube and the QTF plane was ~20 μm [90]. The overall length of the AmR, consisting of two tubes, separated by the QTF, was set to half of the sound wavelength λ in order to create a pressure antinode for the QTF prong spacing [4]. However, the presence of a QTF between the two $\lambda/4$ AmR tubes distorts the AmR acoustic resonances and reduced the QEPAS signal amplitude [13]. The AmR with an ideal but non-matched tube length acted simply as a confinement of the sound wave and did not exhibit a pronounced resonant behaviour. The pressure distribution profiles in AmRs are shown in Fig. 3. Two perfect first longitudinal resonances for two independent $\lambda/2$ tubes are generated when the two tubes are separated and where each tube behaves as an independent resonator, as shown in Fig. 3(a). When the two tubes are attached, the tube pair behaves as a single half-wavelength AmR with a full length of $\lambda/2$ (see Fig. 3(d)). Their gap is approximately equal to the thickness of the QTF crystal, ~200 μm and the two resonators become coupled and the pressure profiles overlap (see Fig. 3(b)). Such an overlapped pressure profile corresponds to a sound pressure distribution in the on-beam QEPAS configuration. The optimum length of each tube is between $\lambda/4$ and $\lambda/2$. Therefore, an optimized AmR tube can produce quasi-resonant standing sound waves in the AmR and significantly improve the QEPAS spectrophone performance [91,95]. In an optimized configuration, the QEPAS detection sensitivity in terms of signal-to-noise ratio (SNR) increases ~30 times when the AmR tubes with the inner diameter of 0.6 mm are cut to a 4.4 mm length in order to match the QTF resonance frequency at pressures between 400 and 800 Torr [13].

The laser focus position h (see Fig. 2(b)) has an impact on the QEPAS signal amplitude and phase. In order to maximize the moment of force but avoid that the sound waves leak from

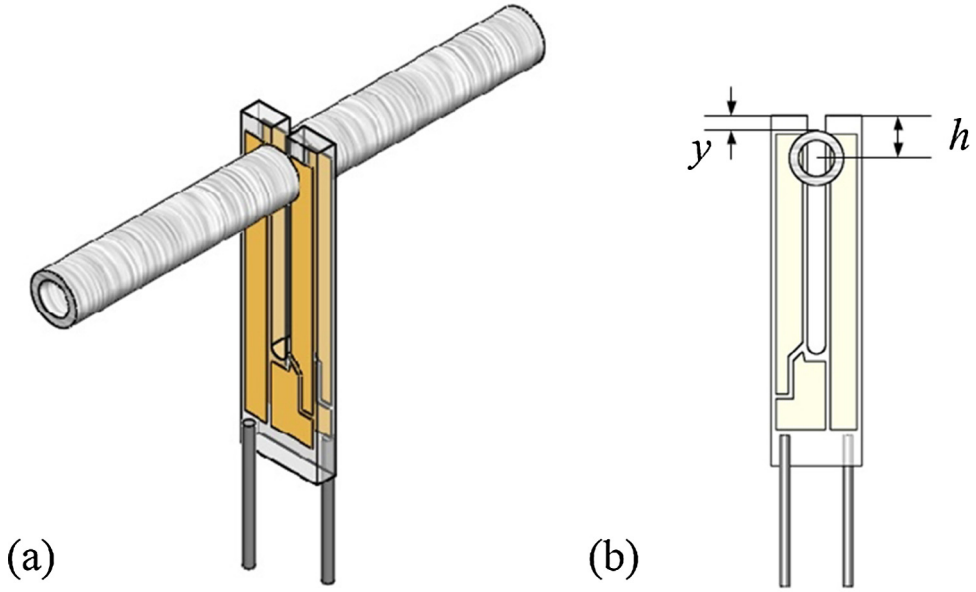

Fig. 2. Schematic diagram of an on-beam QEPAS spectrophone.

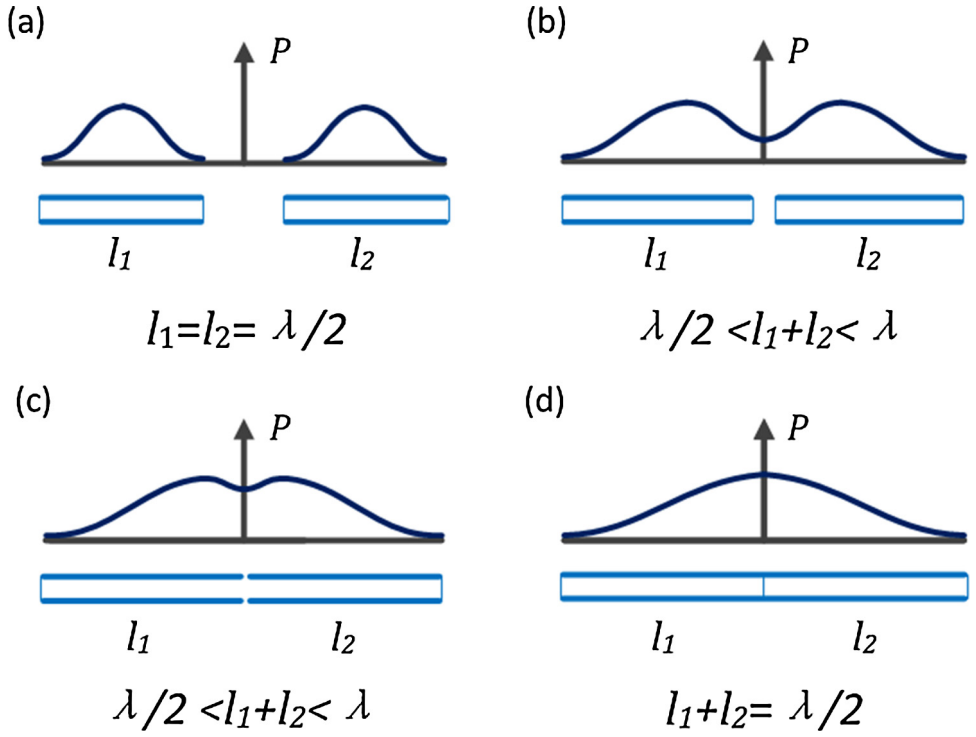

Fig. 3. Sound wave pressure distribution profiles in the AmRs [110].

the QTF prong spacing, the optimal laser focus position with respect to the QTF opening was investigated using a bare QTF without an AmR, which shows an optimal h of ~0.7 mm [92]. However, the coupling effect between the QTF and AmR changes the optimal laser focus position h for a bare QTF. An experiment was implemented to scan the AmR position of the on-beam QEPAS spectrophone along the QTF symmetry axis in order to study the position effect of the AmR. The obtained QEPAS detection SNR indicated that an optimal position to configure the AmR is not h = 0.7 mm, but a flat peak area between y = 0.06 and y = 1.36 mm, as shown in Fig. 4 [93].

A double AmR QEPAS spectrophone was developed by Dong, based on the fact that there is a wide sensitive area along the QTF prong that is sufficient to accommodate two sets of AmRs [96]. The double AmR spectrophone configuration employed two AmRs to construct two detection channels according to the 'on-beam' QEPAS approach, as depicted in Fig. 5. Each AmR was formed by two thin stainless tubes and was coupled to the QTF via excited sound waves in the gas contained inside the AmR tubes. The double AmRs provided two independent detection channels that allow optical signal addition or cancellation and facilitated rapid multi-gas sensing measurements. Energy combination of two lasers

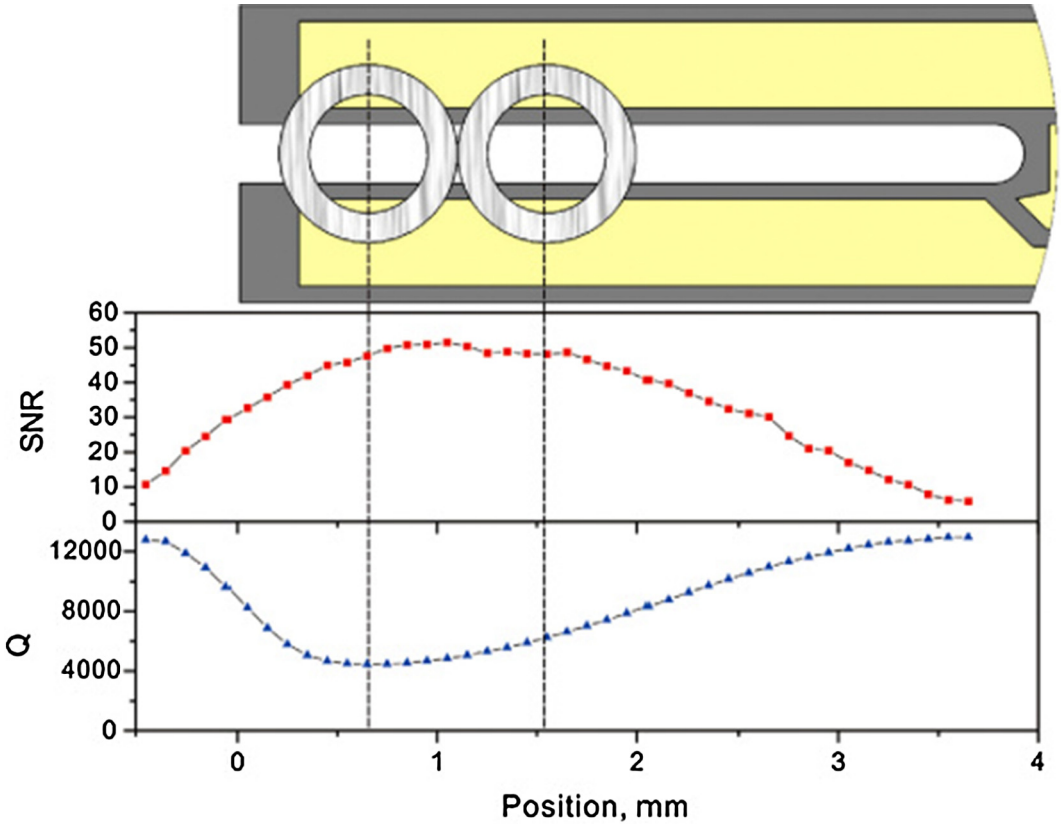

Fig. 4. QEPAS detection SNR as a function of the position y for different AmRs [96].

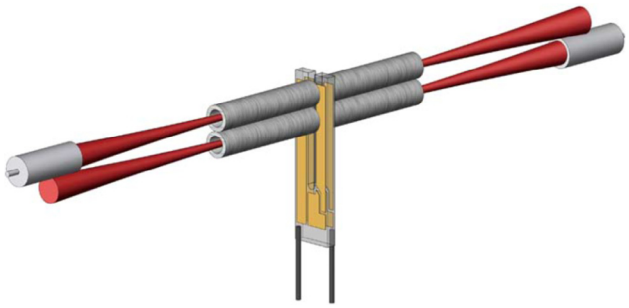

Fig. 5. Schematic diagram of a double AmR QEPAS spectrophone [96].

was demonstrated by using two distributed feedback (DFB) lasers to excite the two AmRs simultaneously for H_2O detection. Two laser beams passed through the two AmRs from both sides, respectively, thereby avoiding laser beam combination. The double AmR spectrophone configuration exhibited a strong acoustic coupling between the AmR and the QTF, which resulted in a lower Q factor value. Since the QEPAS sensor response time t is proportional to the Q factor $t = Q/f$, the double AmR QEPAS spectrophone resulted in a ~5 ms response time.

As a variation of the double AmR QEPAS spectrophone, a right-angle prism was positioned behind the double AmR QEPAS spectrophone, reflecting the incident laser beam and doubling the optical pass through the QTF prongs to produce a second acoustic excitation [97]. The resonance enhancement factor of each AmR was 16 and 12, respectively, with an AmR inner diameter of 0.48 mm. The performance of the improved double AmR QEPAS spectrophone was enhanced by a factor of 22.4, compared to a bare QTF without an AMR.

3.2. Off-beam QEPAS configuration

An off-beam QEPAS (OB-QEPAS) spectrophone configuration, depicted in Fig. 6, was theoretically and experimentally investigated by Liu and Yi [98–100]. In the OB-QEPAS spectrophone, the laser beam is directed through a novel AmR with a slit in the middle and the QTF is placed adjacent to the AmR for the off-beam detection of the sound waves induced by the photoacoustic effect in the AmR. According to the one-dimensional sound wave theory, the antinode of the sound wave longitudinal mode is located at the middle of the AmR with respect to an ideal AmR length of $\sim\lambda/2$. The QTF was placed as close as possible to the slit of the AmR, but avoiding the QTF contacting the AmR in order to maximize the coupling of the sound energy.

Detection of water vapour absorption in air was performed for optimization and evaluation of the OB-QEPAS spectrophone. Dependence of the OB-QEPAS signal upon the AmR length L and the inner diameter (ID) was experimentally investigated. The AmR tubes with the ID ranging from 0.45 to 1.5 mm assembled in the OB-QEPAS configuration were studied. The obtained optimal ID-L ratio R can be calculated from the empirical expression $R = -0.04546 + 0.232 \times ID$. A maximum QEPAS signal was obtained when the AmR was positioned ~0.7 to 1 mm below the QTF opening. The distance between the AmR and the QTF and the tube shape are optimized for detection sensitivity enhancement. The OB-QEPAS has a 1.6–1.7 times lower detection sensitivity than that of the on-beam QEPAS [99]. However the OB-QEPAS configuration is more flexible in terms of the QTF geometry. The OB-QEPAS spectrophone is usually used in the application of broadband laser diodes (LDs) or light emitting diodes (LEDs) [14–16], fibre erbium doped fibre amplifier (EDFA) [101], and mid-infrared laser sources [31,37].

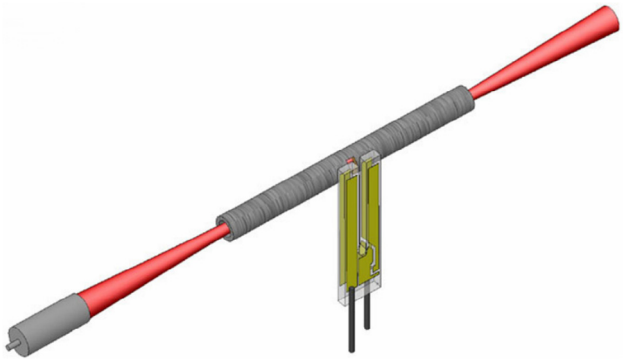

Fig. 6. Schematic diagram of an off-beam QEPAS spectrophone [13].

The off-beam QEPAS configuration has an alternative T-shape QEPAS spectrophone configuration, which was theoretically analysed and experimentally investigated by Yi [102,103]. The T-shape QEPAS spectrophone consists of a long main tube and a short branch tube as shown in Fig. 7. The short branch tube is perpendicularly intersected by the main tube in the middle. The QTF is placed at the end of the branch tube to acquire the photoacoustic waves in the off-beam configuration. An optimized geometry design of the T-shape AmR produced a high acoustic coupling efficiency, with the *Q* factor of the QEPAS spectrophone decreasing from ~10,000 (for a bare QTF) to ~5000 (for the T shape QEPAS spectrophone). The QEPAS spectrophone based on a T-shape AmR improves the detection sensitivity by a factor of >30 with respect to a bare QTF, which is comparable to the on-beam QEPAS spectrophone, while keeping the advantages of the off-beam QEPAS spectrophone. A 3.38 μm distributed feedback laser in combination with a QEPAS spectrophone based on T-shape AmR, capable of simultaneous monitoring of multi-species, was reported by Yi [103].

3.3. Multi-QTF QEPAS configuration

A multi-QTF enhanced QEPAS (M-QEPAS) spectrophone, depicted in Fig. 8, consisting of two QTFs was first reported by Ma [104]. Instead of a single QTF in traditional QEPAS spectrophone, an M-QEPAS spectrophone was developed to increase the signal strength by the superposition of QEPAS signals obtained by each QTF. In the M-QEPAS spectrophone, the two QTFs were mounted in parallel and in opposite directions for a convenient spatial arrangement. In order to evaluate the performance of the M-QEPAS spectrophone, a 1.39 μm DFB laser was used to target a H_2O absorption line. The resonance frequency of the multi-QTF is 32757.3 Hz which is the compromise between QTF_1 ~ 32756.9 Hz and QTF_2 ~ 32757.9 Hz. The *Q* factors of QTF_1, QTF_2 and multi-QTF spectrophone are 5939, 5898 and 5327, respectively.

The impact of distance between the two QTFs on the QEPAS signal amplitude and phase was studied and shown in Fig. 9. With increasing distance between the two QTFs, the QEPAS signal amplitude and phase increase. When the distance was >600 μm, the QEPAS signal was no longer impacted by the distance between the two QTFs. The observed phase shift can be attributed to the coupling of the acoustic wave fields between the two QTFs. The optimized M-QEPAS spectrophone demonstrated a signal amplitude of 1.32 mV which is 1.7 times higher than that of QTF_1 and QTF_2.

The M-QEPAS spectrophone with an on-beam configuration was reported by Zheng et al. [105]. Two types of AmRs were added to the multi-QTF based QEPAS spectrophone to enhance the signal amplitude and were experimentally investigated as shown in Fig. 10. In Fig. 10(a), two QTFs were positioned in parallel with a gap distance of 20 μm. Two stainless steel tubes were positioned closely on the one side of each QTF assembled in the on-beam configuration. The distance from each QTF opening to the center of the AmR was 0.7 mm. In Fig. 10(b), an additional QTF was added to a traditional on-beam spectrophone. The two kinds of QEPAS spectrophone based on multi-QTF show comparable performance when detecting atmospheric H_2O and a signal enhancement of 1.6 times compared to the traditional on-beam QEPAS spectrophone based on a single QTF.

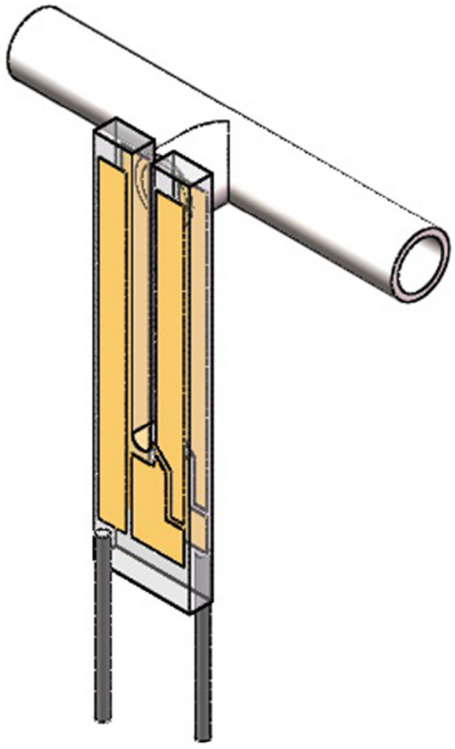

Fig. 7. Schematic diagram of the T-shape QEPAS spectrophone.

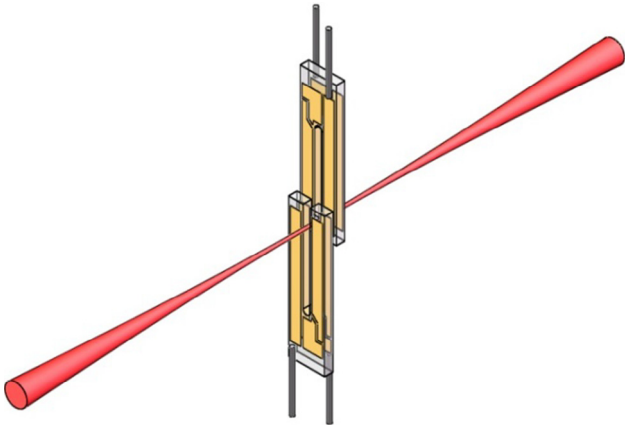

Fig. 8. Schematic diagram of the multi-QTF enhanced QEPAS spectrophone.

4. QEPAS spectrophone employing a custom QTF

One of the technical issues of the QEPAS technique is that the excitation laser beam must 'clearly' pass through the ~300 μm prong spacing of commercially available standard QTFs. In 2013,

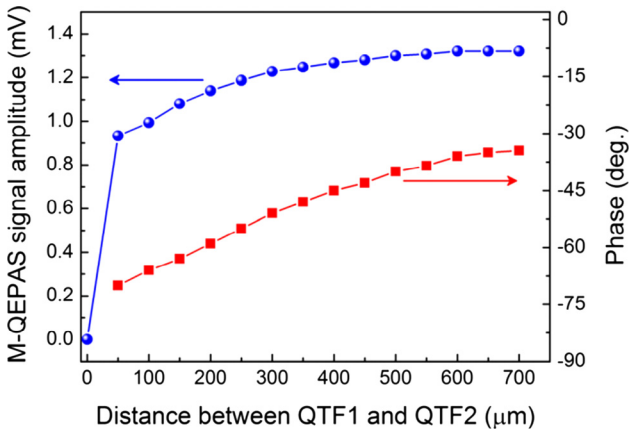

Fig. 9. QEPAS signal amplitude and phase as a function of distance between two QTFs [104].

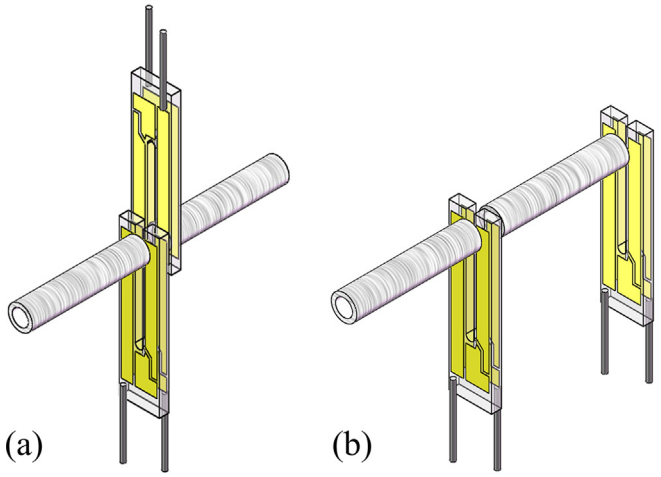

Fig. 10. Schematic diagram of the multi-QTF enhanced on-beam QEPAS spectrophone [105].

a custom-made QTF with a prong spacing of 1 mm was employed in a QEPAS sensor operated in the THz wavelength by Borri and Spagnolo et al. [47]. Due to the long wavelength and the larger beam spatial shape of THz laser sources, it was challenging to collimate the THz beam through the standard QTF prong spacing without touching the QTF. Hence, custom QTFs with larger prong spacing were designed to accommodate THz laser sources [106–108].

4.1. On-beam QEPAS configuration for custom QTFs

A QEPAS spectrophone employing a custom QTF with a prong spacing of ~800 μm assembled in an on-beam configuration was first reported by Wu et al. [109]. Standard photolithographic techniques were used to etch the custom QTF, starting from z-cut quartz wafer. Chromium/gold contacts were deposited on both sides of the QTF. The custom QTF has similar geometry of standard commercial QTF but possesses a ~5 times larger size. A comparison of the QTF geometrical and electrical parameters is shown in Table 1.

Similar to the traditional on-beam QEPAS spectrophone based on a standard QTF (see Fig. 2(a)), a pair of stainless steel tubes with an inner diameter of 1.3 mm was assembled with a custom QTF. The optimum vertical working distance h from the QTF opening to the center of the AmR (see Fig. 2(b)) was 1.2 mm. The expected optimum AmR length was between the $\lambda/4$ and $\lambda/2$, where the sound wavelength λ is ~47 mm calculated from the custom QTF resonance frequency of 7.2 kHz. The performance of a QEPAS spectrophone with an AmR length that varied from 8.4 mm to 23 mm was evaluated. When the overall length of the AmR reached 46 mm, the detection sensitivity of the spectrophone was enhanced ~40-fold compared to a bare custom QTF without an AmR. However, the overall length of the AmR is close to $\sim\lambda$ = 47 mm, which is >5 times longer than the AmR used in the traditional on-beam QEPAS spectrophone based on a standard QTF.

4.2. Single-tube on-beam QEPAS configuration for custom QTFs

A QEPAS spectrophone with a single-tube AmR inserted between the prongs of the custom QTF was developed by Zheng et al. [110]. The single–tube on-beam QEPAS (SO-QEPAS) configuration is shown in Fig. 11. The SO-QEPAS spectrophone configuration can be implemented because of the large prong spacing of the custom QTF to accommodate the AmR and thus avoiding the cutting of the AmR into two pieces. The prong spacing of the used QTF was ~800 μm and the waist of the AmR was machined to <800 μm. A sharp blade was used to open a pair of slits with a width of ~90 μm on each side of the tube waist symmetrically in the middle of the AmR where the acoustic pressure antinode is located.

Fig. 3(c) depicts the pressure distribution profile of the SO-QEPAS AmR. Compared to the on-beam QEPAS spectrophone with the pressure distribution shown in Fig. 3(b), the behaviour of the SO-QEPAS AmR is similar to that of an ideal one dimensional acoustic resonator. By avoiding the use of two independent resonator tubes, a higher acoustic coupling efficiency and a higher sound wave pressure in the QTF prong spacing were obtained. The AmR outer/inner diameters and lengths were optimized for three different resonators. An AmR with an outer diameter of 0.9 mm (which is larger than the QTF prong spacing), an inner diameter of 0.65 mm (which is smaller than the QTF prong spacing) and a length of 38 mm has the optimum sensor performance. The obtained optimum detection SNR compared to the bare custom QTF has a gain factor of 128. With respect to a traditional on-beam spectrophone with a 46 mm AmR, the SO-QEPAS significantly reduces the spectrophone size by 17%, thereby facilitating the laser beam alignment.

4.3. Overtone resonance enhancement of custom QTFs

The resonance frequencies f_n of a QTF in-plane flexural mode can be related to its geometrical parameters and quartz properties by the following equation:

$$f_n = \frac{\pi T}{8\sqrt{12}L^2}\sqrt{\frac{E}{\rho}}n^2 \tag{3}$$

where ρ, E, L, T are the density, Young's modulus, length and width of the QTF, respectively. When n is 1.194 and 2.988, f_n corresponds to the fundamental and first overtone resonance frequency, respectively. A QTF with a prong length L = 17 mm and prong spacing of 700 μm was designed and the fundamental resonance frequency of the QTF was reduced to ~3 kHz, which is one order of magnitude < the resonance frequency of a standard QTF. The ~3 kHz fundamental resonance frequency resulted in a low first overtone resonance frequency of 17.7 kHz. Electro-elastic QTF characterization showed that the QTF geometry design provides a high Q factor of 31,373, when operating in the first overtone resonance, which is ~2.5 times higher than that when operating in fundamental resonance. Based on the above-mentioned fact, a QEPAS spectrophone

Table 1
Geometrical and electrical parameters of a custom QTF and a standard QTF.

	Prong parameters			Electrical parameters		
	Spacing (μm)	Length (mm)	Width (mm)	Frequency (Hz)	Q factor	Resistance (kΩ)
Standard QTF	0.3	3.8	0.6	32,768	12,000	120
Custom QTF	0.8	10	0.9	7205	8536	286

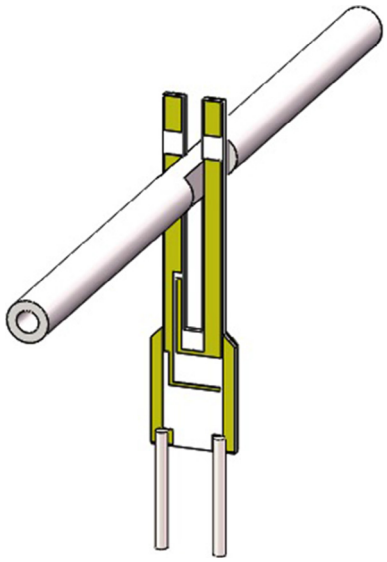

Fig. 11. Schematic diagram of the single tube on-beam QEPAS spectrophone [110].

based on a custom QTF operated in the first overtone resonance mode was developed by Sampaolo et al. [111]. To evaluate the QTF acousto-electric energy conversion efficiency, a DFB laser was used to target the H_2O absorption line in the near-IR wavelength range. The laser beam was focused between the QTF prongs by a lens with a focal length of 40 mm and the laser focal position was scanned along the QTF symmetry axis. The obtained QEPAS signal amplitude versus the laser focus position d is shown in Fig. 12. For the fundamental resonance, the signal amplitude showed a normalized peak value of ~0.18 at d = 15 mm. However, for the first overtone resonance, the signal amplitude showed two peak values at d = 7.5 mm and 15 mm respectively and the amplitude obtained at d = 7.5 mm was ~5.3 times larger than the peak value obtained by the QTF fundamental resonance.

An overtone resonance enhanced single-tube on-beam QEPAS was developed by Zheng et al. by assembling a single tube AmR at the first overtone resonance antinodes of the custom QTF [112]. Due to the high overtone resonance frequency, the optimal AmR length was 14.5 mm, only 5 mm longer than that of a commercial 32 kHz QTF.

A dual gas QEPAS spectrophone was developed by Wu et al. to use only one QTF in order to detect two different gases simultaneously [113]. The realization of dual gas detection was based on the frequency division multiplexing of the QTF fundamental and first overtone resonance frequencies. As shown in Fig. 13, two lasers whose emitting wavelength targeted C_2H_2 and H_2O respectively was used to simultaneously excite a custom QTF. The two lasers were focused at d = 15 mm and 7.5 mm which corresponds to the two vibration antinode points for the fundamental resonance and the first overtone resonance mode, respectively [114]. The output of the QTF was directed to a transimpedance pre-amplifier with a resistance of 10 MΩ and then processed by two lock-in amplifiers connected in parallel for 2*f* detection. The two lock-in amplifiers demodulated the QEPAS signal in the fundamental resonance frequency and first overtone resonance frequency, respectively, to retrieve the information of the two absorbing gas analytes. As a result, dual gas detection of 500 ppm C_2H_2 and a 1.6% water vapour gas mixture in pure N_2 was realized by the dual gas QEPAS spectrophone based on the frequency division multiplexing technique.

4.4. Double-antinode excitation for custom QTFs

A double antinode excited QEPAS (DAE-QEPAS) spectrophone employing a custom QTF operated in the first overtone resonance

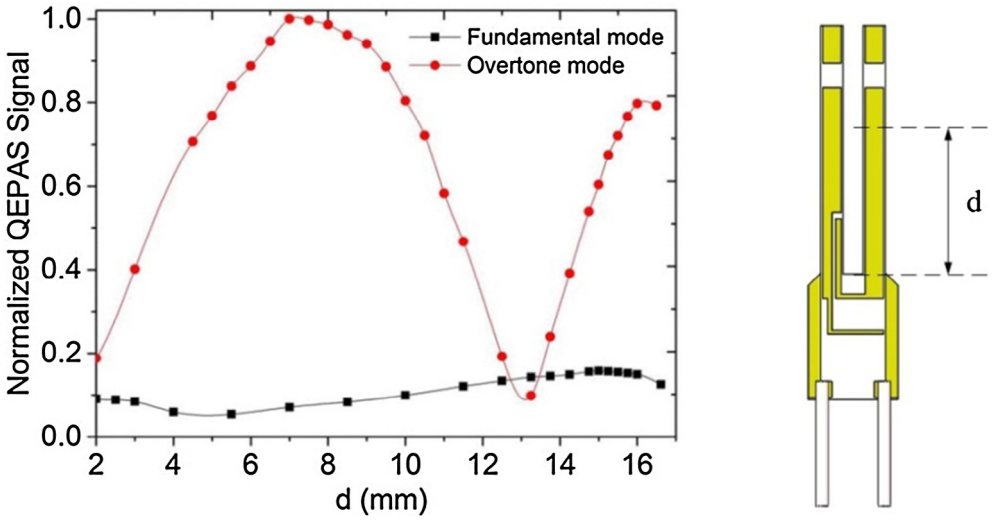

Fig. 12. QEPAS signal amplitude as a function of laser focus distance d from the QTF support [111].

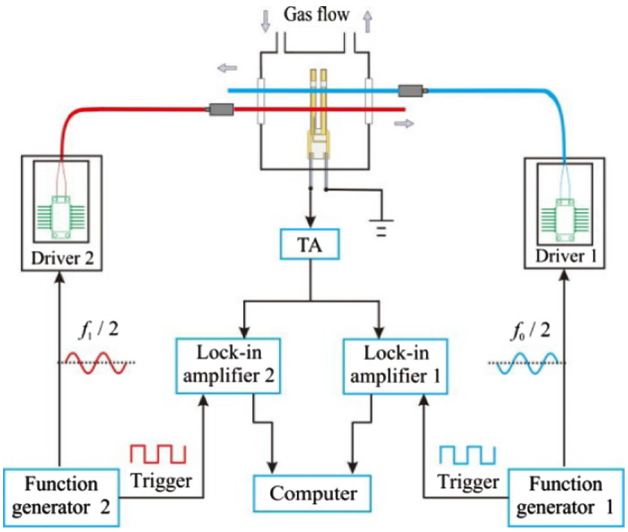

Fig. 13. Schematic of a dual-gas QEPAS sensor system based on a QTF combined vibration in fundamental and 1st overtone resonance modes. TA: transimpedance amplifier [113].

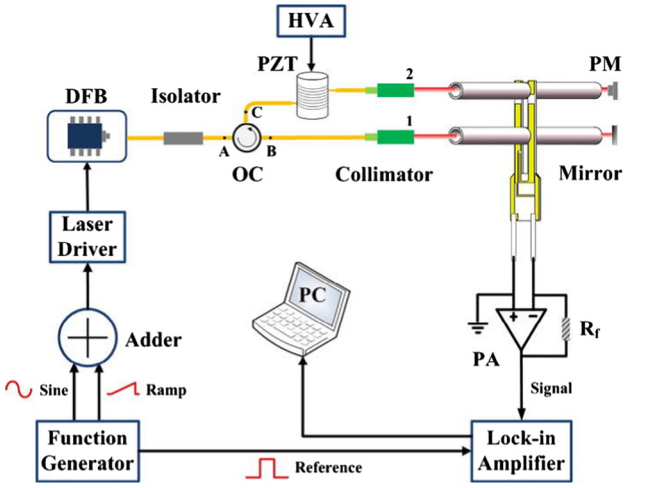

Fig. 14. Schematic of the DAE-QEPAS experimental setup [115]. OC: optical circulator; PZT: piezoelectric transducer; HVA: high voltage amplifier; PM: power meter; PA: pre-amplifier.

mode was reported by Zheng [115]. Two sets of AmR were configured at two antinodes of the QTF first overtone resonance. A reflector and an optical fibre circulator were employed to realize three optical passes by using only a single laser source. The experimental setup is depicted in Fig. 14.

A 1.37 μm DFB laser was employed to target an H_2O absorption line to evaluate the spectrophone performance. A fiber coiled piezoelectric transducer (PZT) was used to compensate the phase shift between the two antinodes. Two thin stainless steel tubes were assembled in an on-beam configuration at two antinodes of the QTF first overtone resonance. With an AmR inner diameter of 1.3 mm, a length of 8.5 mm, the DAE-QEPAS spectrophone realized a *Q* factor of 7790 with respect to the bare QTF *Q* factor of 12,770 and attained a detection sensitivity of ~100 times with respect to that of a single antinode excited bare custom QTF without an AmR. The DAE-QEPAS configuration minimized the spectrophone power consumption as well as opened a new approach for optical balanced detection.

5. Conclusions

This paper is a review of the development of QEPAS spectrophones employing both commercially available standard QTFs as well as custom made QTFs. The review of the QEPAS spectrophone employing standard QTFs focused on both on-beam and off-beam mode AmR configurations. The on-beam spectrophone configuration allowed the laser beam to pass through the QTF prong spacing in order to produce a sound source between the QTF prongs. A pair of AmR was assembled perpendicularly to the QTF plane to confine the sound waves. Both the AmR diameters and length influenced the spectrophone performance. The optimization was studied both theoretically and experimentally in order to improve the on-beam QEPAS spectrophone. For the off-beam spectrophone configuration the advantage is that the QTF is positioned adjacent to the AmR. The off-beam spectrophone configuration enables the laser photoacoustic effect to generate sound waves to drive the QTF prongs without passing through the QTF prong spacing and which therefore simplifies laser beam alignment. However the acoustic coupling efficiency of the off-beam spectrophone configuration was found to be lower than the on-beam spectrophone configuration. Custom QTFs with >2 times larger prong spacing and lower resonance frequency than standard QTFs were designed in order to eliminate the requirement of high laser beam quality. By use of custom QTFs, laser sources with limited beam quality, such as THz laser sources and broadband laser diodes, were applied to the QEPAS spectrophone. Benefiting from the large prong spacing of the custom QTF, an AmR was assembled for the custom QTF in the on-beam configuration in order to achieve a higher spectrophone performance. A challenge to the QEPAS spectrophone employing custom QTFs was caused by the low resonance frequency of custom QTFs. A lower resonance frequency *f* resulted in a longer sound wavelength λ, which meant a longer AmR, which reduced the advantage of a custom QTF in laser beam alignment. The single-tube, on-beam QEPAS configuration effectively solved the challenge of a large prong spacing and a lower resonance frequency of a custom QTF. The large prong spacing of the custom QTF accommodated a single tube AmR inserted between the QTF prongs, avoiding separating a tube into pieces in a conventional on-beam QEPAS configuration. Due to the more effective resonance coupling effect between the QTF and the AmR, the use of a single tube AmR not only reduces the AmR length but also enhances the detection sensitivity of the QEPAS spectrophone. A new custom QTF design enabled the use of a QTF overtone resonance vibration resulting in improved QEPAS spectrophone performance. The lower fundamental resonance frequency of a lower overtone resonance of ~17 kHz was suitable for trace gas detection. The optimized QTF geometry design made it possible that the *Q* factor of the QTF's first overtone resonance was two times higher than its fundamental resonance. The combination of the single-tube on-beam configuration and the QTF overtone resonance enhancement resulted in an improved QEPAS detection sensitivity and a more compact spectrophone structure. The excitation of two antinodes of the QTF's first overtone resonance can further improve the QEPAS spectrophone performance. A frequency division multiplexing technique based on the QTF combined vibration of the fundamental and first overtone resonance modes was developed for simultaneous dual gas detection. Another effective way to boost the QEPAS detection sensitivity significantly is to couple the QTF into a high-finesse power build-up cavity [116–118]. Improvement in detection sensitive can be made by optimization of the octupole gold pattern configuration of the QTF. Furthermore, an optimized custom QTF can be used in calibration-free beat frequency QEPAS for measuring ultra-low gas concentration levels with short aver-

aging times by detecting the beat frequency signal of the QTF and demodulating the signal at a non-resonance frequency of the QTF [119].

Acknowledgements

The Shanxi University team acknowledges support by National Key Research and Development Program of China (No. 2017YFA0304203); National Natural Science Foundation of China (Grants #61622503, 61575113); Changjiang Scholars and Innovative Research Team in University of Ministry of Education of China (No. IRT13076); the Outstanding Innovative Teams of Higher Learning Institutions of Shanxi and Shanxi '1331 Project' key subjects construction. Frank K. Tittel acknowledges support by the Welch Foundation (Grant R4925U).

References

[1] J.M. Friedt, E. Carry, Am. J. Phys. 75 (2007) 415.
[2] A.A. Kosterev, Y.A. Bakhirkin, R.F. Curl, F.K. Tittel, Opt. Lett. 27 (2002) 1902.
[3] P. Patimisco, G. Scamarcio, F.K. Tittel, V. Spagnolo, Sensors 14 (2014) 6165.
[4] A.A. Kosterev, F.K. Tittel, D.V. Serebryakov, A.L. Malinovsky, I.V. Morozov, Rev. Sci. Instrum. 76 (2005) 043105.
[5] G. Wysocki, A.A. Kosterev, F.K. Tittel, Appl. Phys. B 85 (2006) 301.
[6] X. Yin, L. Dong, H. Zheng, X. Liu, H. Wu, Y. Yang, W. Ma, W. Ma, L. Zhang, W. Yin, L. Xiao, S. Jia, Sensors 16 (2016) 162.
[7] A.A. Kosterev, Y.A. Bakhirkin, F.K. Tittel, S. McWhorter, B. Ashcraft, Appl. Phys. B 92 (2008) 103.
[8] H. Zheng, M. Lou, L. Dong, H. Wu, W. Ye, X. Yin, C.S. Kim, M. Kim, W.W. Bewley, C.D. Merritt, C.L. Canedy, M.V. Warren, I. Vurgaftman, J.R. Meyer, F.K. Tittel, Opt. Expr. 25 (2017) 16761.
[9] X. Yin, L. Dong, H. Wu, H. Zheng, W. Ma, L. Zhang, W. Yin, S. Jia, F.K. Tittel, Sens. Actuators B 247 (2017) 329.
[10] Z. Bozóki, A. Pogany, G. Szabo, Appl. Spectrosc. Rev 46 (2011) 1.
[11] A. Elia, C. Di Franco, P.M. Lugarà, G. Scamarcio, Sensors 6 (2006) 1411.
[12] A. Schmohl, A. Miklós, P. Hess, Appl. Opt. 41 (2002) 1815.
[13] L. Dong, A.A. Kosterev, D. Thomazy, F.K. Tittel, Appl. Phys. B 100 (2010) 627.
[14] S. Böttger, M. Köhring, U. Willer, W. Schade, Appl. Phys. B 113 (2013) 227.
[15] H. Yi, K. Liu, W. Chen, T. Tan, L. Wang, X. Gao, Opt. Lett. 36 (2011) 481.
[16] H. Zheng, L. Dong, Y. Ma, H. Wu, X. Liu, X. Yin, L. Zhang, W. Ma, W. Yin, L. Xiao, S. Jia, Opt. Expr. 24 (2016) A752.
[17] H. Zheng, L. Dong, X. Yin, X. Liu, H. Wu, L. Zhang, W. Ma, W. Yin, S. Jia, Sens. Actuators B 208 (2015) 173.
[18] S. Schilt, A.A. Kosterev, F.K. Tittel, Appl. Phys. B 95 (2009) 813.
[19] H. Wu, L. Dong, X. Liu, H. Zheng, X. Yin, W. Ma, L. Zhang, W. Yin, S. Jia, Sensors 15 (2015) 26743.
[20] A. Elia, P.M. Lugarà, C. Di Franco, V. Spagnolo, Sensors 9 (2009) 9616.
[21] Y. Cao, W. Jin, H.L. Ho, Proc. SPIE 8439 (2012) 843928.
[22] A.A. Kosterev, F.K. Tittel, Appl. Opt. 43 (2004) 6213.
[23] P. Gong, L. Xie, X. Qi, R. Wang, IEEE Photon. Technol. Lett. 27 (2015) 545.
[24] K. Liu, W. Zhao, L. Wang, G. Wang, W. Zhang, X. Gao, W. Chen, Opt. Commun. 340 (2015) 126.
[25] R. Lewicki, G. Wysocki, A.A. Kosterev, F.K. Tittel, Appl. Phys. B 87 (2007) 157.
[26] Y. Ma, G. Yu, J. Zhang, X. Yu, R. Sun, J. Optics 17 (2015) 055401.
[27] M. Jahjah, A. Vicet, Y. Rouillard, Appl. Phys. B 106 (2012) 483.
[28] S. Viciani, M.S. de Cumis, S. Borri, P. Patimisco, A. Sampaolo, G. Scamarcio, P. De Natale, F. D'Amato, V. Spagnolo, Appl. Phys. B 119 (1) (2015) 21.
[29] T. Nguyen Ba, M. Triki, G. Desbrosses, A. Vicet, Rev. Sci. Instrum. 86 (2015) 023111.
[30] M. Jahjah, S. Belahsene, L. Nähle, M. Fischer, J. Koeth, Y. Rouillard, A. Vicet, Opt. Lett. 37 (2012) 2502.
[31] J.P. Waclawek, R. Lewicki, H. Moser, M. Brandstetter, F.K. Tittel, B. Lendl, Appl. Phys. B 117 (2014) 113.
[32] S. Gray, A. Liu, F. Xie, C. Zah, Opt. Expr. 18 (2010) 23353.
[33] M. Lassen, L. Lamard, Y. Feng, A. Peremans, J.C. Petersen, Opt. Lett. 41 (2016) 4118.
[34] M. Triki, T.N. Ba, A. Vicet, Inf. Phys. Technol. 69 (2015) 74.
[35] V. Spagnolo, P. Patimisco, S. Borri, G. Scamarcio, B.E. Bernacki, J. Kriesel, Appl. Phys. B 112 (2013) 25.
[36] M. Helman, H. Moser, A. Dudkowiak, B. Lendl, Appl. Phys. B 123 (2017) 141.
[37] Z. Li, C. Shi, W. Ren, Opt. Lett. 41 (2016) 4095.
[38] J.P. Waclawek, H. Moser, B. Lendl, Opt. Expr. 24 (2016) 6559.
[39] Z. Wang, Z. Li, W. Ren, Opt. Expr. 24 (2016) 4143.
[40] T. Rück, R. Bierl, F.M. Matysik, 255 Sens. Actuators B (2018) 2462.
[41] V. Spagnolo, P. Patimisco, S. Borri, G. Scamarcio, B.E. Bernacki, J. Kriesel, Opt. Lett. 37 (2012) 4461.
[42] D. Weidmann, A.A. Kosterev, F.K. Tittel, N. Ryan, D. McDonald, Opt. Lett. 29 (2004) 1837.
[43] V. Spagnolo, A.A. Kosterev, L. Dong, R. Lewicki, F.K. Tittel, Appl. Phys. B 100 (2010) 125.
[44] A.K.Y. Ngai, S.T. Persijn, I.D. Lindsay, A.A. Kosterev, P. Groß, C.J. Lee, S.M. Cristescu, F.K. Tittel, K.J. Boller, F.J.M. Harren, Appl. Phys. B 89 (2007) 123.
[45] A.A. Kosterev, Y.A. Bakhirkin, F.K. Tittel, Appl. Phys. B 80 (2005) 133.
[46] L. Dong, R. Lewicki, K. Liu, P.R. Buerki, M.J. Weida, F.K. Tittel, Appl. Phys. B 107 (2012) 275.
[47] S. Borri, P. Patimisco, A. Sampaolo, H.E. Beere, D.A. Ritchie, M.S. Vitiello, G. Scamarcio, V. Spagnolo, Appl. Phys. Lett. 103 (2013) 021105.
[48] P. Patimisco, S. Borri, A. Sampaolo, H.E. Beere, D.A. Ritchie, M.S. Vitiello, G. Scamarcio, V. Spagnolo, Analyst 139 (2014) 2079.
[49] A. Sampaolo, P. Patimisco, M. Giglio, M.S. Vitiello, H.E. Beere, D.A. Ritchie, G. Scamarcio, F.K. Tittel, V. Spagnolo, Sensors 16 (2016) 439.
[50] V. Spagnolo, P. Patimisco, R. Pennetta, A. Sampaolo, G. Scamarcio, M.S. Vitiello, F.K. Tittel, Opt. Expr. 23 (2015) 7582.
[51] P. Stefański, R. Lewicki, N.P. Sanchez, J. Tarka, R.J. Griffin, M. Razeghi, F.K. Tittel, Appl. Phys. B 117 (2014) 519.
[52] Y. Ma, R. Lewicki, M. Razeghi, F.K. Tittel, Opt. Expr. 21 (2013) 1008.
[53] M.S. de Cumis, S. Viciani, S. Borri, P. Patimisco, A. Sampaolo, G. Scamarcio, P. De Natale, F. D'Amato, V. Spagnolo, Opt. Expr. 22 (2014) 28222.
[54] H. Zheng, L. Dong, X. Liu, Y. Liu, H. Wu, W. Ma, L. Zhang, W. Yin, S. Jia, Laser Phys. 25 (2015) 125601.
[55] M. Jahjah, W. Jiang, N.P. Sanchez, W. Ren, P. Patimisco, V. Spagnolo, S.C. Herndon, R.J. Griffin, F.K. Tittel, Opt. Lett. 39 (2014) 957.
[56] D. Kumar, S. Gupta, S. Kumar, R.C. Sharma, R.K. Soni, Spectrosc. Lett. 49 (2016) 469.
[57] P. Gong, L. Xie, X. Qi, R. Wang, H. Wang, Mi. Chang, H. Yang, F. Sun, G. Li, Chin. Phys. B 24 (2015) 014206.
[58] D.V. Serebryakov, I.V. Morozov, A.A. Kosterev, V.S. Letokhov, Quant. Electron. 40 (2010) 167.
[59] J. Petersen, L. Lamard, P. Feng, J.F. Focant, A. Peremansb, M. Lassen, Proc. SPIE 10055 (2017) 1005503.
[60] R. Lewicki, A.A. Kosterev, D.M. Thomazy, T.H. Risby, S. Solga, T.B. Schwartz, F. K. Tittel, Proc. SPIE 7945 (2011) 7945K–1.
[61] M. Lassen, L. Lamar, P. Feng, A. Peremans, J.C. Petersen, in: CLEO: Science and Innovations. Optical Society of America, 2017 SF1M.4.
[62] A.A. Kosterev, F.K. Tittel, G. Bearman, Int. J. Aerosp. Eng. 1 (2009) 331.
[63] A. Sampaolo, P. Patimisco, M. Giglio, L. Chieco, G. Scamarcio, F.K. Tittel, V. Spagnolo, Opt. Expr. 24 (2016) 15872.
[64] A. Nedjalkov, J. Meyer, M. Köhring, A. Doering, M. Angelmahr, S. Dahle, A. Sander, A. Fischer, W. Schade, Batteries 2 (2016) 5.
[65] V. Spagnolo, L. Dong, A.A. Kosterev, D. Thomazy, J.H. Doty, F.K. Tittel, Opt. Lett. 36 (2011) 460.
[66] A.A. Kosterev, L. Dong, D. Thomazy, F.K. Tittel, S. Overby, Appl. Phys. B 101 (2010) 649.
[67] A.A. Kosterev, P.R. Buerki, L. Dong, M. Reed, T. Day, F.K. Tittel, Appl. Phys. B 100 (2010) 173.
[68] V. Spagnolo, L. Dong, A.A. Kosterev, D. Thomazy, J.H. Doty III, F.K. Tittel, Appl. Phys. B 103 (2011) 735.
[69] Z. Wang, J. Geng, W. Ren, Appl. Spectrosc. 71 (2017) 1834.
[70] M. Mordmueller, W. Schade, U. Willer, Appl. Phys. B 123 (2017) 224.
[71] Z. Wang, Q. Wang, J.Y.L. Ching, J.C.Y. Wu, G. Zhang, W. Ren, Sens. Actuators B 246 (2017) 710.
[72] W. Schippers, M. Köhring, S. Böttger, U. Willer, G. Flachenecker, W. Schade, Appl. Phys. B 116 (2014) 53.
[73] C. Bauer, U. Willer, R. Lewicki, A. Pohlkötter, A.A. Kosterev, D. Kosynkin, F.K. Tittel, W. Schade, J. Phys.: Conf. Ser. 157 (2009) 012002.
[74] R. Lewicki, G. Wysocki, A.A. Kosterev, F.K. Tittel, Opt. Expr. 15 (2007) 7357.
[75] L. Dong, A.A. Kosterev, D. Thomazy, F.K. Tittel, Proc. SPIE 7945 (2011) 79450R–1.
[76] W. Ren, W. Jiang, N.P. Sanchez, P. Patimisco, V. Spagnolo, C. Zah, F. Xie, L.C. Hughes, R.J. Griffin, F.K. Tittel, Appl. Phys. Lett. 104 (2014) 041117.
[77] R.C. Sharma, D. Kumar, N. Bhardwaj, A.K. Maini, Curr. Sci. India 104 (2013) 1548.
[78] H. Yi, R. Maamary, X. Gao, M.W. Sigrist, E. Fertein, W. Chen, Appl. Phys. Lett. 106 (2015) 101109.
[79] A. Pohlkötter, M. Köhring, U. Willer, W. Schade, Sensors 10 (2010) 8466.
[80] P. Patimisco, A. Sampaolo, Y. Bidaux, A. Bismuto, M. Scott, J. Jiang, A. Muller, J. Faist, F.K. Tittel, V. Spagnolo, Opt. Expr. 24 (2016) 25943.
[81] T. Starecki, P.Z. Wieczorek, Sensors 17 (2017) 2528.
[82] F. Wang, J. Chang, Q. Wang, Y. Liu, Z. Liu, Z. Qin, C. Zhu, Opt. Commun. 381 (2016) 152.
[83] Y. Dong, J. Chen, L. Luo, E. Forsberg, S. He, C. Yan, Appl. Opt. 54 (2015) 4202.
[84] Y. Ma, G. Yu, J. Zhang, X. Yu, R. Sun, F.K. Tittel, Sensors 15 (2015) 7596.
[85] Y. Ma, Y. He, X. Yu, J. Zhang, R. Sun, F.K. Tittel, Appl. Phys. Lett. 108 (2016) 091115.
[86] Y. Ma, Y. He, X. Yua, C. Chen, R. Sun, F.K. Tittel, Sens. Actuators B 233 (2016) 388.
[87] Y. Ma, Y. He, Y. Tong, X. Yu, F.K. Tittel, Opt. Expr. 25 (2017) 29356.
[88] Y. Ma, Y. He, L. Zhang, X. Yu, J. Zhang, R. Sun, F.K. Tittel, Appl. Phys. Lett. 110 (2017) 031107.
[89] A. Miklós, P. Hess, Rev. Sci. Instrum. 72 (2001) 1937.
[90] Y. Cao, W. Jin, H.L. Ho, Sens. Actuators B 174 (2012) 24.
[91] G. Aous, R. Levy, M. Raybaut, A. Godard, J. Melkonian, M. Lefebvre, Appl. Phys. B 123 (2017) 63.
[92] N. Petra, J. Zweck, A.A. Kosterev, S.E. Minkoff, D. Thomazy, Appl. Phys. B 94 (2009) 673.

[93] H. Wu, L. Dong, W. Ren, W. Yin, W. Ma, L. Zhang, S. Jia, F.K. Tittel, Sens. Actuators B 206 (2015) 364.
[94] K. Liu, J. Li, L. Wang, T. Tan, W. Zhang, X. Gao, W. Chen, F.K. Tittel, Appl. Phys. B 94 (2009) 527.
[95] H. Yi, W. Chen, X. Guo, S. Sun, K. Liu, T. Tan, W. Zhang, X. Gao, Appl. Phys. B 108 (2012) 361.
[96] L. Dong, H. Wu, H. Zheng, Y. Liu, X. Liu, W. Jiang, L. Zhang, W. Ma, W. Ren, W. Yin, S. Jia, F.K. Tittel, Opt. Lett. 39 (2014) 2479.
[97] Y. Liu, J. Chang, J. Lian, Z. Liu, Q. Wang, Z. Qin, Sensors 16 (2016) 214.
[98] K. Liu, X. Guo, H. Yi, W. Chen, W. Zhang, X. Gao, Opt. Lett. 34 (2009) 1594.
[99] K. Liu, H. Yi, A.A. Kosterev, W. Chen, L. Dong, L. Wang, T. Tan, W. Zhang, F.K. Tittel, X. Guo, Rev. Sci. Instrum. 81 (2010) 103103.
[100] H. Yi, K. Liu, S. Sun, W. Zhang, X. Gao, Opt. Commun. 285 (2012) 5306.
[101] H. Wu, L. Dong, H. Zheng, X. Liu, X. Yin, W. Ma, L. Zhang, W. Yin, S. Jia, F.K. Tittel, Sens. Actuators, B 221 (2015) 666.
[102] H. Yi, W. Chen, S. Sun, K. Liu, T. Tan, X. Gao, Opt. Expr. 20 (2012) 9187.
[103] H. Yi, W. Chen, A. Vicet, Z. Cao, X. Gao, T. Nguyen-ba, M. Gahjah, Y. Rouillard, L. Nähle, M. Fischer, Appl. Phys. B. 116 (2014) 423.
[104] Y. Ma, X. Yu, G. Yu, X. Li, J. Zhang, D. Chen, R. Sun, F.K. Tittel, App. Phys. Lett. 107 (2015) 021106.
[105] H. Zheng, X. Yin, L. Dong, H. Wu, X. Liu, W. Ma, L. Zhang, W. Yin, S. Jia, J. Spectrosc. (2015).
[106] P. Patimisco, A. Sampaolo, H. Zheng, L. Dong, F.K. Tittel, V. Spagnolo, Adv. Phys. X 2 (2017) 169.
[107] G. Aoust, R. Levy, M. Raybaut, J. -M. Melkonian, B. Bourgeteau, A. Godard, M. Lefebvre, in: 2016 Conference on. IEEE, 2016.
[108] P. Patimisco, A. Sampaolo, L. Dong, M. Giglio, G. Scamarcio, F.K. Tittel, V. Spagnolo, Sens. Actuators, B 227 (2016) 539.
[109] H. Wu, A. Sampaolo, L. Dong, P. Patimisco, X. Liu, H. Zheng, X. Yin, W. Ma, L. Zhang, W. Yin, V. Spagnolo, S. Jia, F.K. Tittel, App. Phys. Lett. 107 (2015) 111104.
[110] H. Zheng, L. Dong, A. Sampaolo, H. Wu, P. Patimisco, X. Yin, W. Ma, L. Zhang, W. Yin, V. Spagnolo, S. Jia, F.K. Tittel, Opt. Lett. 41 (2016) 978.
[111] A. Sampaolo, P. Patimsco, L. Dong, A. Geras, G. Scamarcio, T. Starecki, F.K. Tittel, V. Spagnolo, Appl. Phys. Lett. 107 (2015) 231102.
[112] H. Zheng, L. Dong, A. Sampaolo, P. Patimisco, W. Ma, L. Zhang, W. Yin, L. Xiao, V. Spagnolo, S. Jia, F.K. Tittel, Appl. Phys. Lett. 109 (2016) 111103.
[113] H. Wu, X. Yin, L. Dong, K. Pei, A. Sampaolo, P. Patimisco, H. Zheng, W. Ma, L. Zhang, W. Yin, L. Xiao, V. Spagnolo, S. Jia, F.K. Tittel, Appl. Phys. Lett. 110 (2017) 121104.
[114] F.K. Tittel, A. Sampaolo, P. Patimisco, L. Dong, A. Geras, T. Starecki, V. Spagnolo, Opt. Expr. 24 (2016) A682.
[115] H. Zheng, L. Dong, P. Patimisco, H. Wu, A. Sampaolo, X. Yin, S. Li, W. Ma, L. Zhang, W. Yin, L. Xiao, V. Spagnolo, S. Jia, F.K. Tittel, Appl. Phys. Lett. 110 (2017) 021110.
[116] P. Patimisco, S. Borri, L. Galli, D. Mazzotti, G. Giufredi, N. Akikusa, M. Yamanishi, G. Scamarcio, P.D. Natale, V. Spagnolo, Analyst 140 (2015) 736.
[117] P. Patimisco, A. Sampaolo, F.K. Tittel, V. Spagnolo, Sensor Actuators A 267 (2017) 70.
[118] J. Wojtas, A. Gluszek, A. Hudzikowski, F.K. Tittel, Sensors 17 (2017) 513.
[119] H. Wu, L. Dong, H. Zheng, Y. Yu, W. Ma, L. Zhang, W. Yin, L. Xiao, S. Jia, F.K. Tittel, Nat. Commun. 8 (2017) 15331.

Huadan Zheng received his B.S. degree in physics from Shanxi University, China, in 2012. He is now pursuing a Ph.D. degree of atomic and molecular physics from the Institute of Laser Spectroscopy at Shanxi University. From August, 2016 to September, 2017, he worked as a visiting research student in the Electrical and Computer Engineering Department, Rice University, Houston, USA. His research interests include gas sensors, photoacoustic spectroscopy, and laser spectroscopy techniques.

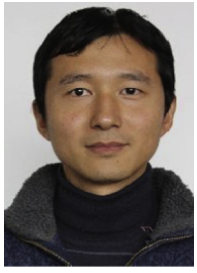

Lei Dong received his Ph.D. degree in optics from Shanxi University, China in 2007. From June, 2008 to December, 2011, he worked as a post-doctoral fellow in the Electrical and Computer Engineering Department and Rice Quantum Institute, Rice University, Houston, USA. Currently he is a professor in the Institute of Laser Spectroscopy of Shanxi University. His research interests include optical sensors, trace gas detection, and laser spectroscopy.

Hongpeng Wu received his B.S. degree in physics from Shanxi University, China in 2011. He is now a lecturer at Institute of Laser Spectroscopy, Shanxi University. From August, 2015 to September, 2016, he worked as a research visiting student in the Electrical and Computer Engineering Department, Rice University, Houston, USA. His research interests include tunable diode laser absorption spectroscopy, photoacoustic spectroscopy and laser spectroscopy techniques.

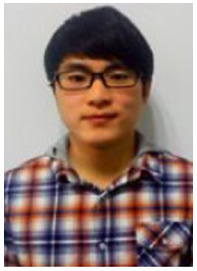

Xukun Yin received his B.S. degree in physics from Shanxi University, China, in 2014. He is now pursuing a Ph.D. degree in atomic and molecular physics from the Institute of Laser Spectroscopy at Shanxi University. His research interests include gas sensors and photoacoustic spectroscopy.

Liantuan Xiao received his Ph.D. in optics from Shanxi University, China in 2001. He worked as a visiting scholar in Laboratories of SATIE and LPQM of the ENS de CACHAN, France in 2001. He also worked as a visiting professor in Prof. M. Orrit's group, Leiden University, Netherlands in 2008. Now he is a Changjiang scholar of Shanxi University and the director of the Institute for Laser Spectroscopy at Shanxi University. His research interests include laser spectroscopy, single-molecule optics, and optical sensing.

Suotang Jia received his B.S. degree in physics in 1986 and the M.S. degree in optics in 1989 from Shanxi University, China. He graduated in 1994 with a Ph.D. degree from the East China Normal University. Prof. S. Jia was a visiting scholar at the CNRS in France, the University of Maryland, Yale University and the University of Connecticut since 1996. Prof. S. Jia is now a professor at Shanxi University and the President of Shanxi University since 2012. His research interests include quantum optics, quantum information, ultracold atom and molecules as well as applications of laser spectroscopy.

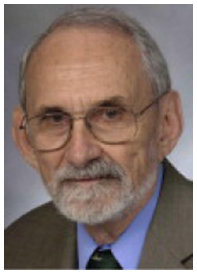

Robert F. Curl is Kenneth S. Pitzer-Schlumberger Professor of Natural Sciences Emeritus and University Professor Emeritus at Rice University. He attended Rice Institute receiving the B.A. from Rice in 1954 and the Ph. D. from Berkeley in 1957. After a postdoctoral at Harvard, he joined the faculty at Rice where he has been ever since. He is a member of the National Academy of Sciences, European Academy of Arts and Sciences, Phi Beta Kappa, Phi Lambda Upsilon, and Sigma Xi. He is a Fellow of the American Academy of Arts and Sciences, a Fellow of the Optical Society of America, Fellow of the Royal Society of Chemistry, and Honorary Fellow of the Royal Society of New Zealand. Jointly with Richard Smalley and Harold Kroto, he received the Nobel Prize in Chemistry in 1996. He has received a number of other awards. His primary research interests have been in molecular spectroscopy, chemical kinetics, and the chemistry of elemental carbon.

Frank K. Tittel received his B.S. degree in physics in 1955 and the Ph.D. degree in physics in 1959 from Oxford University. Now he is the J. S. Abercrombie Professor in the School of Engineering, Rice University, Houston, USA. Professor Frank Tittel has been involved in many innovative developments in quantum electronics and laser technology since the discovery of the laser in 1960, with applications ranging from laser spectroscopy to environmental monitoring. His most recent research utilizes novel quantum cascade and interband cascade lasers to achieve compact, robust instrumentation that can be deployed for various applications, such as air and water quality monitoring relevant to the International Space Station funded by NASA, urban formaldehyde monitoring funded by the Environmental Protection Agency, non-invasive NO and CO detection in biomedical systems funded by the National Institute of Health and the National Science Foundation (http://lasersci.rice.edu/). His current research is funded by the US Department of Energy-Monitor Program, the DOD-Scout Program, and the Welch Foundation.